Supplementary Materials

Microwave-assisted hydrothermal synthesis of space fillers to enhance volumetric energy density of NMC811 cathode material for Li-ion batteries

Irina A. Skvortsova, Aleksandra A. Savina, Elena D. Orlova, Vladislav S. Gorshkov, Artem M. Abakumov

Center for Energy Science and Technology, Skolkovo Institute of Science and Technology, Nobel str. 3, 121205 Moscow

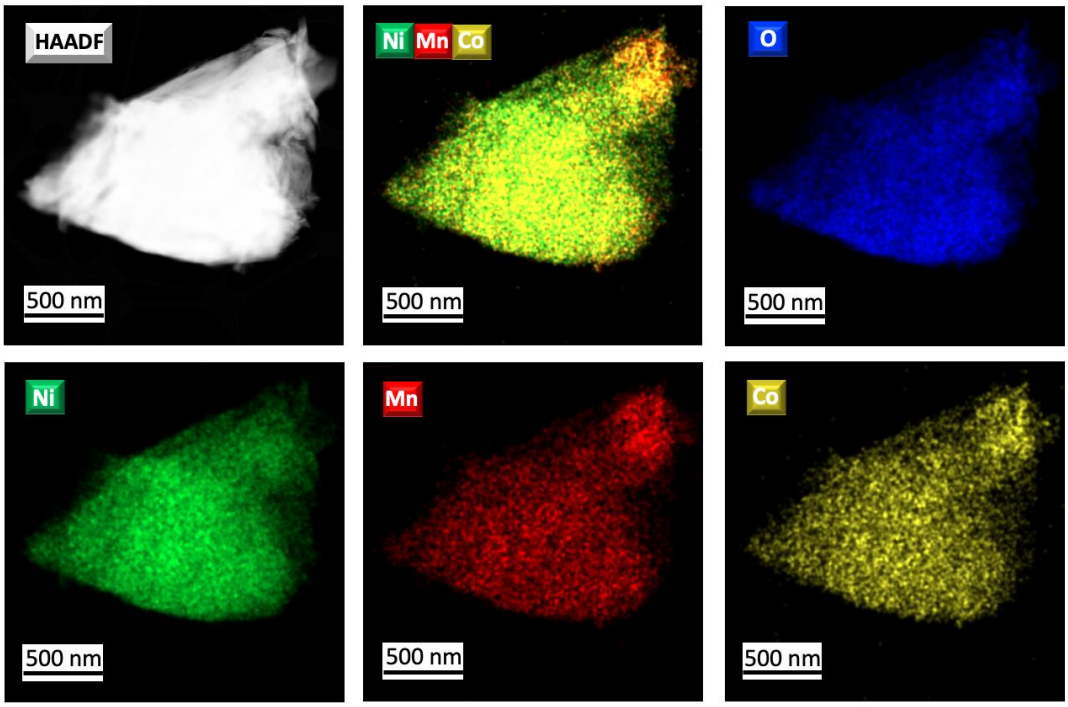

Figure S1. Typical HAADF-STEM images of the $Ni_{0.8}Mn_{0.1}Co_{0.1}(OH)_2$ precursor obtained via a microwave-assisted hydrothermal route with low glycine concentration (TM:Gly molar ratio of 1:12.35) along with color-coded STEM-EDX compositional map and elemental maps of O, Ni, Mn, and Co.

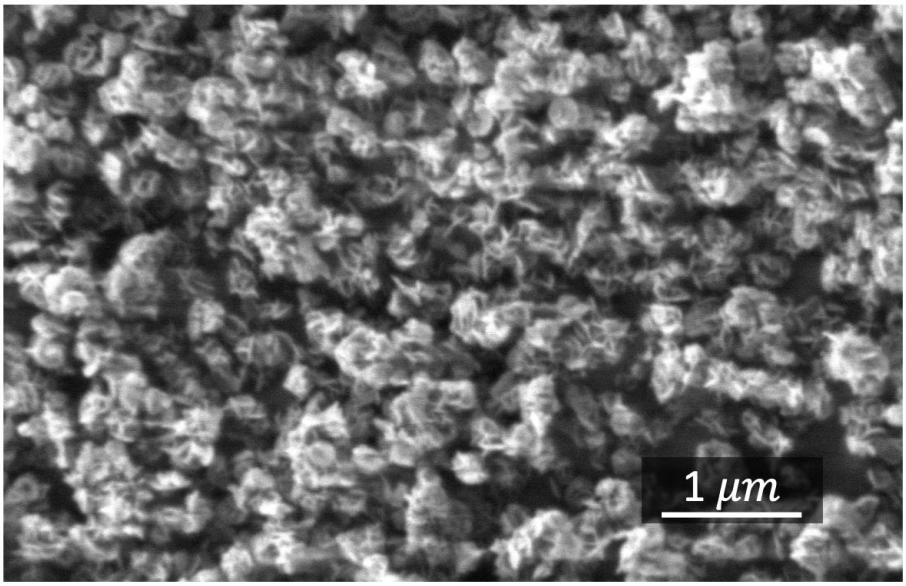

Figure S2. SEM image of $Ni_{0.8}Mn_{0.1}Co_{0.1}(OH)_2$ sample obtained using a microwave-assisted hydrothermal route with low NaOH concentration (TM:NaOH molar ratio of 1:20).

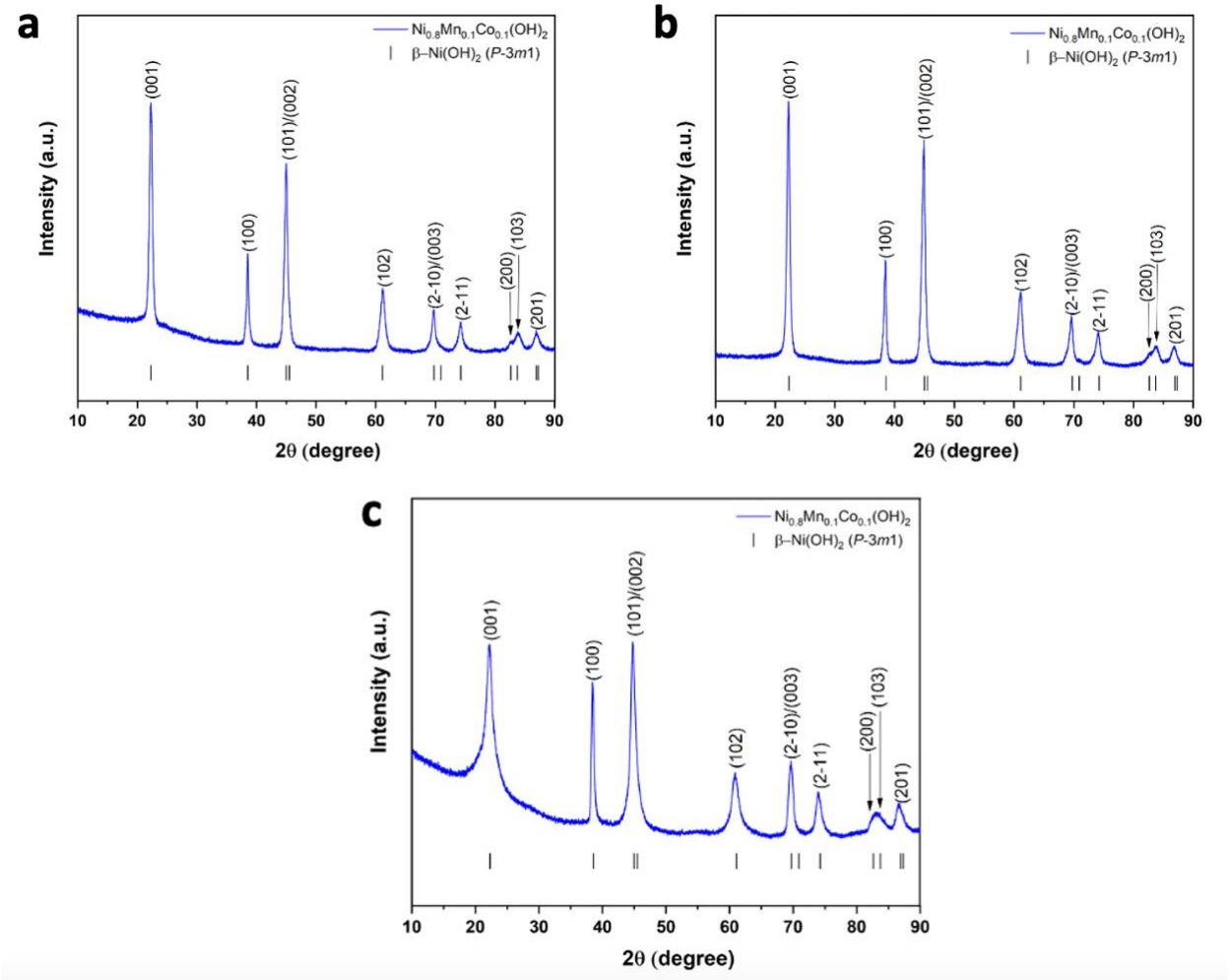

Figure S3. Powder XRD patterns (blue curve) for the $Ni_{0.8}Mn_{0.1}Co_{0.1}(OH)_2$ precursors MW_15m (a = 3.125(1) Å, c = 4.619(2) Å) (a), MW_60m (a = 3.131(5) Å, c = 4.615(1) Å) (b) and CP (a = 3.115(3) Å, c = 4.614(1) Å) (c). Bragg reflection positions for the β-$Ni(OH)_2$ structure are marked with black vertical lines.

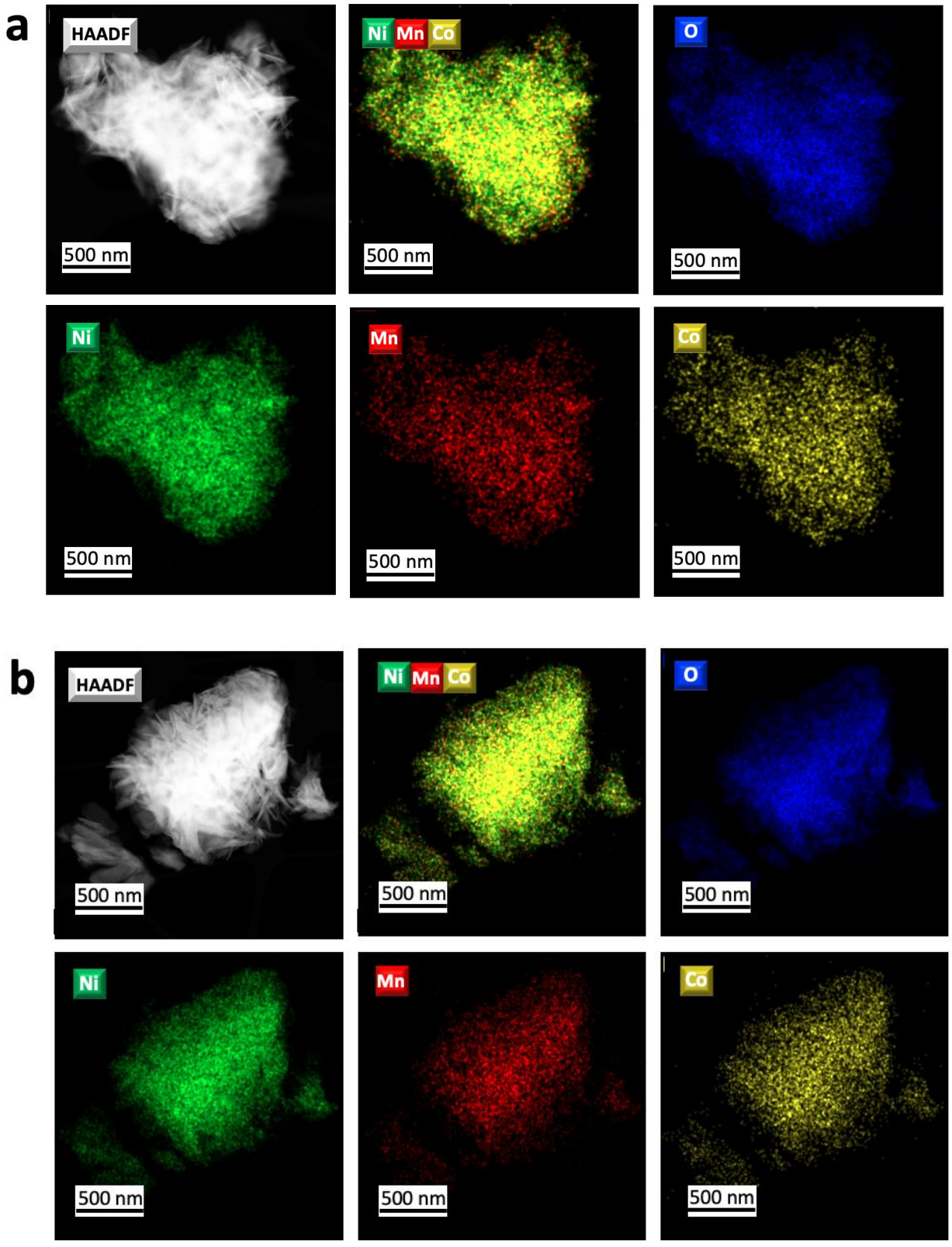

Figure S4. HAADF-STEM images of the MW_15m (a) and MW_60m (b) hydroxide precursors along with the corresponding color-coded STEM-EDX compositional maps and elemental maps of O, Ni, Mn, and Co.

Table S1. Quantitative EDX analysis for the $Ni_{0.8}Mn_{0.1}Co_{0.1}(OH)_2$ precursors.

Sample	Ni, mol. fraction	Mn, mol. fraction	Co, mol. fraction
MW_15m	0.810±0.012	0.110±0.023	0.080±0.019
MW_30m	0.798±0.022	0.086±0.016	0.116±0.011
MW_60m	0.796±0.020	0.084±0.015	0.120±0.021

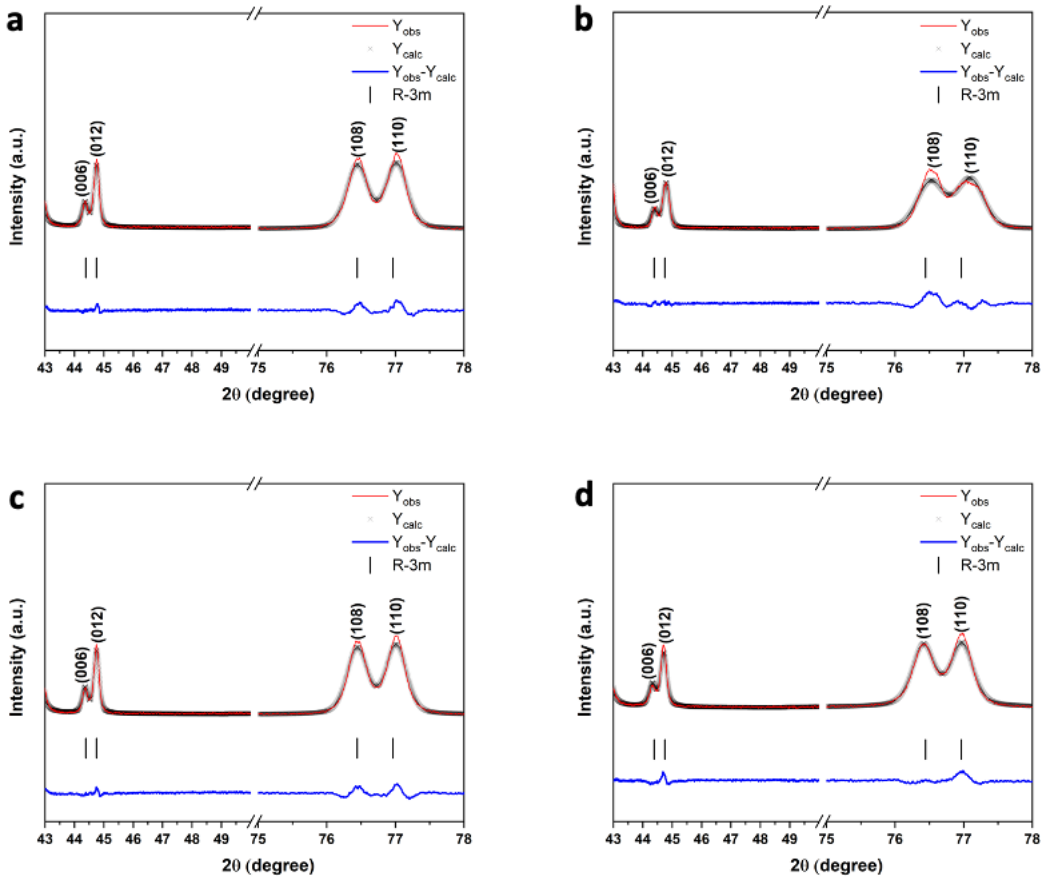

Figure S5. Splitting of (006)/(012) and (108)/(110) peaks on experimental (black), calculated (red), and difference (blue) powder XRD patterns of the MW_15m_A (a), MW_30m_A (b), MW_60m_A (c) and CP_A (d) samples after Rietveld refinement. Bragg reflection positions (sp. gr. $R\bar{3}m$) are marked with black vertical lines.

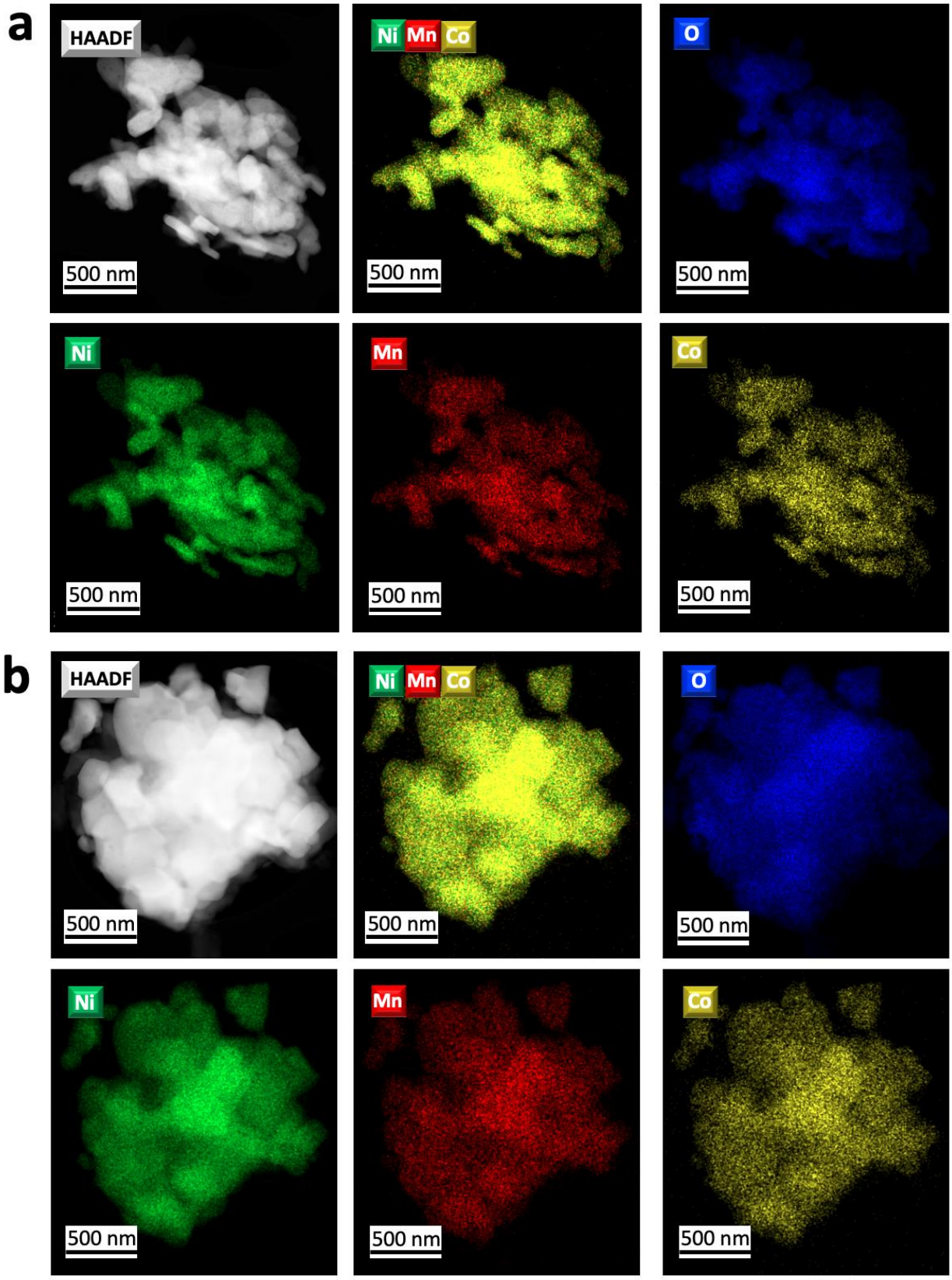

Figure S6. HAADF-STEM images of the MW_15m_A (a) and MW_60m_A (b) NMC811 samples along with the corresponding color-coded STEM-EDX compositional maps and elemental maps of O, Ni, Mn, and Co.

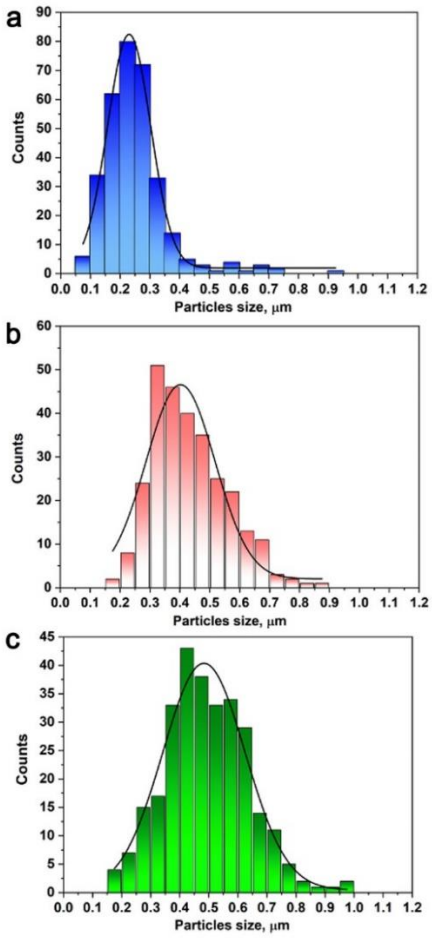

Figure S7. Size distributions of the primary particles in the NMC811 samples MW_15m_A (a), MW_30m_A (b), and MW_60m_A (c).

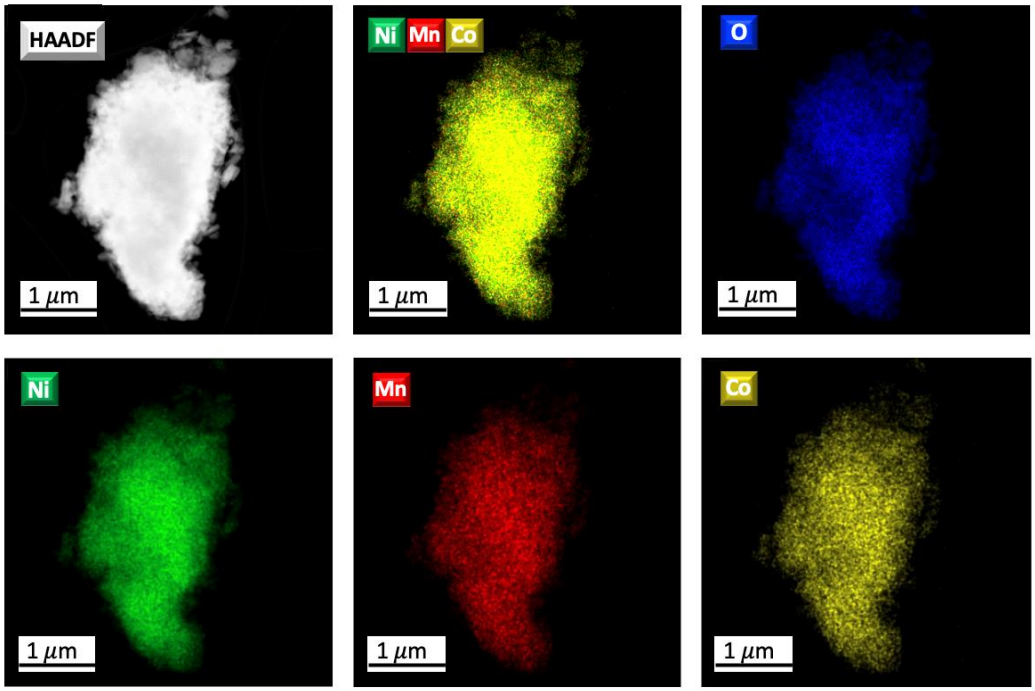

Figure S8. HAADF-STEM image of the CP_A NMC811 sample obtained through coprecipitation route along with the color-coded STEM-EDX compositional map and elemental maps of O, Ni, Mn, and Co.

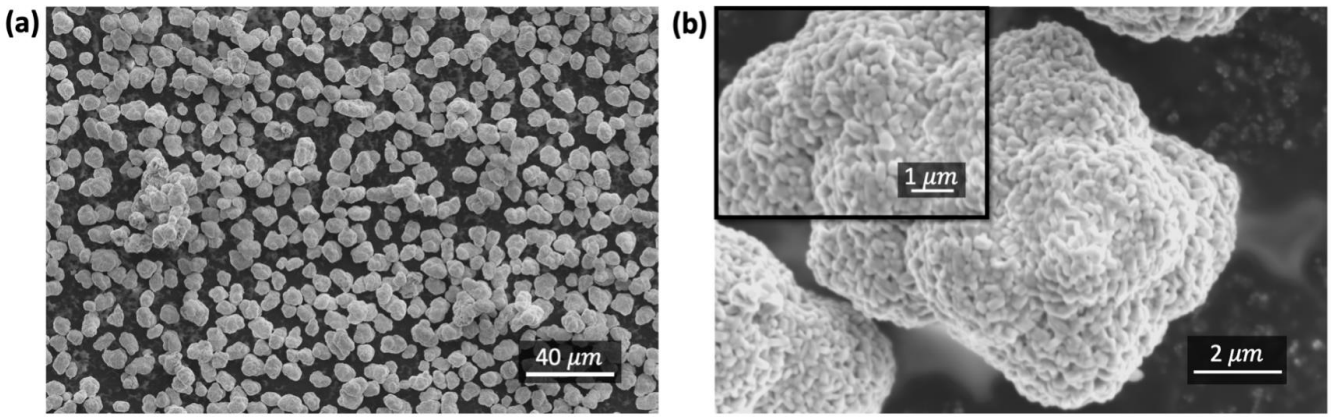

Figure S9. SEM images of the CP_A NMC811 sample obtained through co-precipitation.

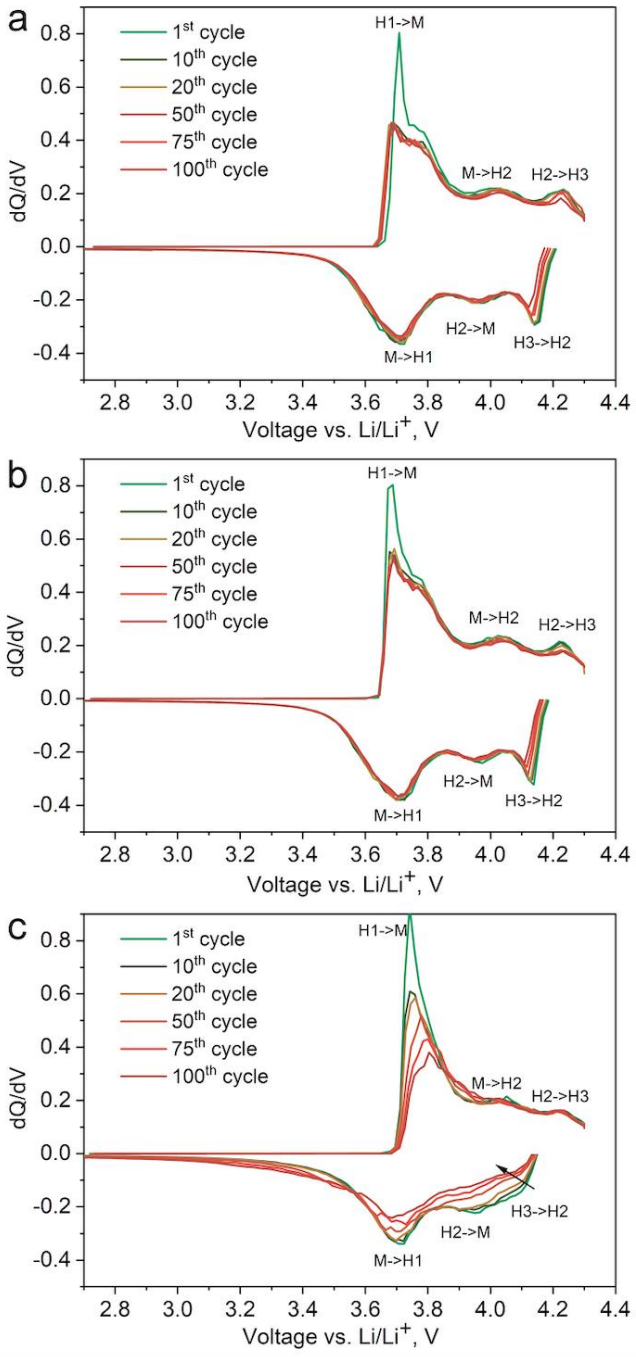

Figure S10. Differential capacity plots for the NMC811 MW_15m_A (a), MW_30m_A (b), and MW_60m_A (c) samples.

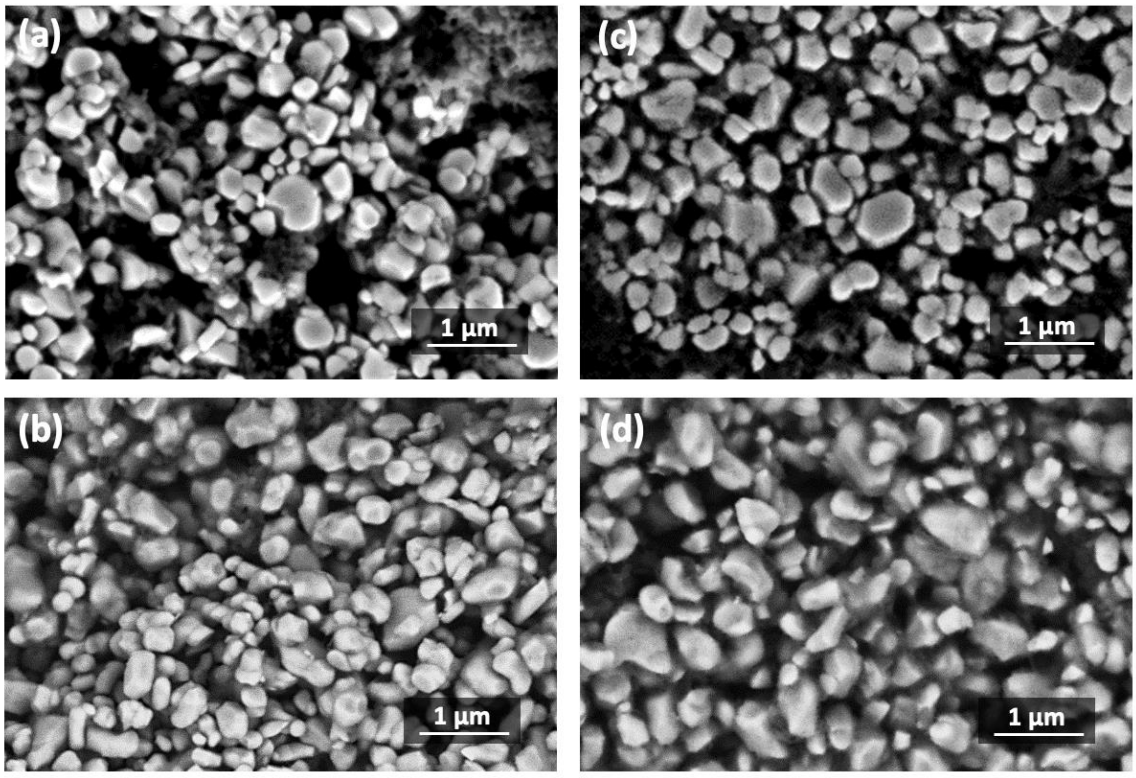

Figure S11. SEM images of the pristine (a,b) and 330 times cycled (c, d) NMC811 electrodes of the MW_15m_A (a,c) and MW_30m_A (b, d) samples.

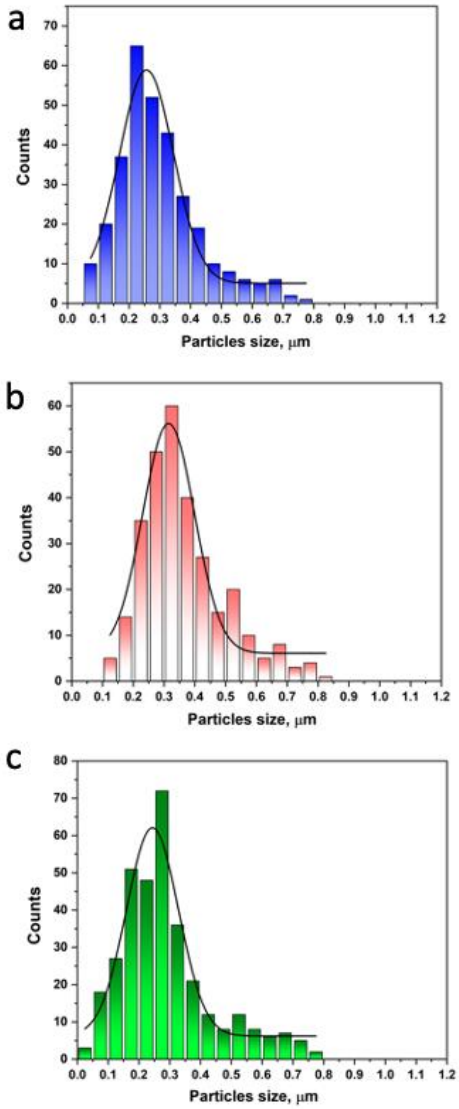

Figure S12. Size distributions of the primary particles in the NMC811 electrodes MW_15m_A (a), MW_30m_A (b), and MW_60m_A (c) after 330 charge/discharge cycles.

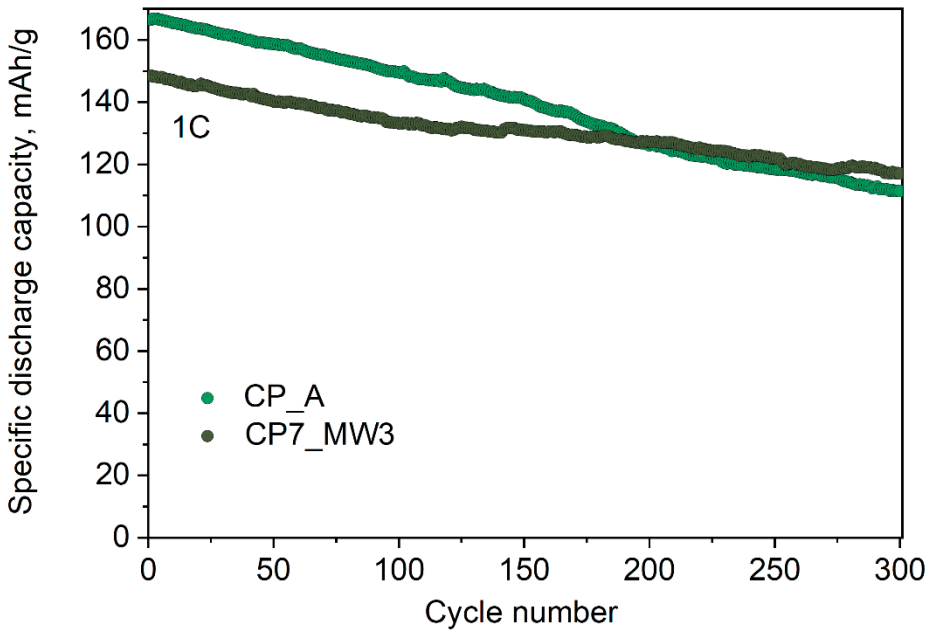

Figure S13. Capacity retention at 1C rate of the CP_A and CP7_MW3 NMC811 samples in half-cells with metallic lithium anode.

Table S2. The results of EIS spectra approximation by a selected equivalent circuit.

CP7_MW3		R_{sol}, Ω	R_{SEI}, Ω	C_{SEI}, F	φ_{SEI}	R_{ct}, Ω	C_{dl}, F	φ_{dl}
	Value	0	34.33	$1.06 \cdot 10^{-5}$	0.91	67.89	$9.61 \cdot 10^{-4}$	0.83
	Accuracy	0	0.69%	2.89%	0.38%	0.45%	1.40%	0.41%
1W_30m_A		R_{sol}, Ω	R_{SEI}, Ω	C_{SEI}, F	φ_{SEI}	R_{ct}, Ω	C_{dl}, F	φ_{dl}
	Value	0	29.49	$1.13 \cdot 10^{-5}$	0.80	48.18	$3.04 \cdot 10^{-3}$	0.83
	Accuracy	0	1.04%	4.40%	0.58%	0.70%	1.69%	0.31%
CP_A		R_{sol}, Ω	R_{SEI}, Ω	C_{SEI}, F	φ_{SEI}	R_{ct}, Ω	C_{dl}, F	φ_{dl}

	Value	1.04	14.22	$1.43 \cdot 10^{-5}$	0.90	85.82	$1.87 \cdot 10^{-3}$	0.86
	Accuracy	0.66%	0.36%	2.54%	0.27%	0.59%	1.05%	0.38%